an additional maximum appears. As the values of X increase, the vibrational velocity component in the ejection phase also decreases and at two tube diameters (X = 0.45 m) small-amplitude random fluctuation of the gas in the core of the jet is observed. Similar behavior of the velocity fluctuations is also observed in narrow tubes ($m \geq 1$). However, the decrease in the oscillatory component in the ejection phase is observed at five diameters [9]. Thus, the experiments have revealed a number of distinctive features of the vibrations of a gas column in an open tube whose diameter is greater than the piston diameter. The results will be useful for investigating the action of an external wave field on mass-transfer processes in gas–liquid systems.

NOTATION

ω_n and ω_n^* are the linear and nonlinear resonance frequencies; a_0 is the speed of sound in the undisturbed gas; L_0 is the length of the tube; L is the reduced length of the tube; d_0 is the piston diameter; d is the tube diameter; $2\ell_0$ is the piston stroke; h is the height of the adapter; V_{max} is the maximum velocity; r is the horizontal displacement; X is the distance in the axial direction.

LITERATURE CITED

1. R. G. Zaripov and M. A. Ilhamov, J. Sound Vibr., 46, No. 2, 245-257 (1976).
2. R. G. Zaripov, Akust. Zh., 23, No. 3, 378-383 (1977).
3. J. Disselhorst and L. Van Wüngaarden, J. Fluid Mech., 99, No. 3, 293-319 (1980).
4. R. G. Galiullin, I. P. Revva, and G. G. Khakimov, Akust. Zh., 28, No. 5, 617-621 (1982).
5. M. Salikuddin and W. H. Broun, J. Sound Vibr., 106, (1), 71-106 (1985).
6. E. Stuhltrager and H. Thomman, ZAMP, 37, No. 3, 155-157 (1986).
7. Sh. U. Galiev, Nonlinear Waves in Finite Continua [in Russian], Kiev (1988).
8. R. G. Galiullin and E. I. Permyakov, Akust. Zh., 34, No. 4, 733-735 (1988).
9. V. B. Repin, Yu. N. Novikov, and A. P. Dement'ev, Unsteady Problems of Mechanics [in Russian], Kazan (1989), pp. 103-110.

HYDRODYNAMICS AND HEAT EXCHANGE IN COOLING SYSTEMS WITH INTERSECTING CHANNELS. I. HYDRODYNAMIC CHARACTERISTICS

Yu. I. Shanin, V. A. Afanas'ev, and O. I. Shanin

UDC 536.35:62-405.8;621.375

We present the results of visualization and measurement of hydrodynamic drag for $Re_1 = 1 \cdot 10^2$-$2.5 \cdot 10^4$ as a function of the geometry and the angle of flow about the structure.

Introduction. One of the goals of using a cooling system with intersecting channels is to increase the rate of heat transfer. There is only one attempt in the literature [1] to generalize the experimental data on the hydraulic drag for such systems. In the case closest to our area of application [2], a structure of considerable relative height ($h_c/\delta_c \sim$ 7-9) was examined, and there were no data on the hydraulic drag. However, in a number of technical objects the thickness of the heat exchanger must be limited.

In the present work we experimentally determine the structure of the flow and the hydraulic drag in cooling systems with intersecting channels of moderate height (h_c/δ_c = 1-3).

Generally the form of such a system (so called waffled structure) is obtained by forming a series of channels of uniform height h_c which intersect each other at angle φ in the material. A series of fins are formed having longitudinal spacing S_2 and transverse spacing S_1, and in the general case the channels can have different widths δ_{c1}, δ_{c2}. In practice,

Translated from Inzhenerno-fizicheskii Zhurnal, Vol. 61, No. 5, pp. 717-725, November, 1991. Original article submitted January 23, 1990.

0022-0841/91/6105-1317$12.50

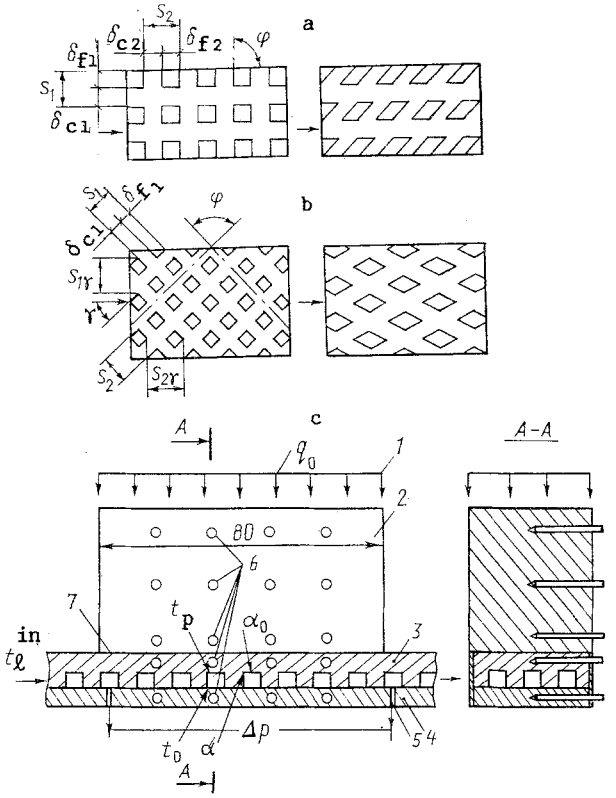

Fig. 1. Plan view of the structure and diagram of the experiment: a) in-step; b) staggered; c) diagram of the experimental section: 1) ohmic heater; 2) thermal wedge; 3) monolithic plate with cooling system; 4) adjoining plate; 5) pressure extraction; 6) thermocouples; 7) indium–gallium eutectic.

mutually perpendicular channels of uniform height are the most commonly realized case (Fig. 1). Under the condition $S_1 = S_2$ the structure consists of fins of square ($\varphi = 90°$) or of rhombic ($\varphi < 90°$) section, and for $S_2 \gg S_1$, depending on the ratio S_2/d_h, the structure can be thought of as a system of extended ($S_2/d_h > 30$) or short ($S_2/d_h < 30$) channels. For heat exchangers which are circular in plan, the case of flow about a waffled structure with angle of attack γ is realized and the spacing characteristics change in accordance with

$$S_{1\gamma} = S_1 \cos\gamma + S_2 \sin\gamma, \quad S_{2\gamma} = S_1 \sin\gamma + S_2 \cos\gamma. \tag{1}$$

The porosity of such a system does not depend on the angle φ. For a variation of the ratio δ_c/δ_f over the range 0.5-2.0 the porosity of the system changes from 0.56 to 0.89, i.e., there is the possibility of adjusting the effect of porosity by the choice of channel spacing and width. In the case of square ($\varphi = 90°$) or rhombic ($60 < \varphi < 90°$, angles $\varphi < 60°$ being difficult to obtain technically) fins, $\varepsilon = 0.75$. In analogy with a tube bundle, for changes in the angle of attack one can select two cases of symmetric flow about the structure: in-line spacing of the fins $\gamma_1 = \varphi + \pi n$, $\gamma_2 = \pi n$, $n = 0, 1, 2, \ldots$; or staggered fin spacing $\gamma_3 = (\varphi/2) + \pi n$, $n = 0, 1, 2, \ldots$; $\gamma_4 = (\varphi/2) + \pi(2n - 1)/2$, $n = 1, 2, \ldots$.

The investigation of the hydraulic characteristics was done on special models made of two plates joined together by diffusive welding or brazing. The cooling system is formed by milling or by electromachining a series of intersecting channels in one of the plates. Some of the models were sandblasted to remove small welding seams, the magnitude of the resultant roughness being R_z = 10-20 μm. The geometric dimensions of the models are given in Table 1. Each model was drained by four ports of 1-mm diameter for sampling of static pressure. These ports were spaced l = 70-80 mm apart, at equal distances from the entry and exit of the model. The side walls of the model were capped with coverings. Supply and discharge receptacles were fastened with flanges attached to the model along its edges. These receptacles consisted of tubes of inner diameter 46 mm and length 180 mm. The fluid entry conditions into the model corresponded to the outflow conditions from a large volume, which ensured a uniform velocity profile at entry. In the fluid channel there were placed air-

TABLE 1. Characteristics of Cooling System Models Studied

Model No.	Model width and height, mm (length 110 mm)	Intersection angle of channels φ, deg	Angle of attack γ, deg	Channel width δ_c, height h_c, mm	Channel hydraulic diam. d_h, mm	Fin width δ_f, mm	Porosity ε	Compactness K, m^2/m^3	Coef. of thermal conductivity for frame material λ, W/(m·K)
1	32; 4,9	90	0	2,0; 2,4	2,18	2,0	0,750	1125	380
2	30; 5,1	90	45	2,0; 2,8	2,33	2,0	0,750	1040	380
3	30; 26	90	0	2,13; 1,90	2,00	1,9	0,780	1284	380
4	30,4; 9	90	15	1,95; 3,05	2,38	2,07	0,735	994	380
5	30,2; 9	90	30	1,92; 2,08	2,37	2,08	0,730	987	380
6	30; 12	90	0	1,64; 1,62	1,63	1,47	0,770	1580	380
7	30; 12	90	15	1,57; 1,76	1,66	1,46	0,770	1510	380
8	30; 12	90	30	1,53; 1,80	1,65	1,44	0,770	1490	380
9	30; 12	90	40	1,57; 1,60	1,58	1,44	0,770	1600	380
10	30; 12	90	45	1,63; 1,73	1,68	1,34	0,796	1530	380
11	30; 12	60	15	1,12; 3,22	1,66	1,27	0,717	1337	130
12	30; 9,4	60	0	1,12; 3,06	1,64	1,26	0,720	1374	130
13	30; 11,3	60	30	1,0; 3,0	1,50	1,51	0,638	1384	380
14	30; 9,2	60	30	1,25; 3,45	1,83	1,24	0,75	1238	130
15	30; 12	60	30	1,13; 3,22	1,86	2,37	0,543	1110	380
16	30; 12	90	0	2,0; 3,0	2,40	2,0	0,750	1000	~1
17	30; 12	90	45	2,4; 3,1	2,29	1,62	0,838	941	~1

inflated containers and the apparatus which regulated and measured flow rate and pressure. The water flow rate at room temperature (t_ℓ = 15-25°C) was measured by direct reading flow meters and turbine flow meters, with a maximum relative error of ±(2.5-3)%, from 1 g/sec to maximum, which was determined by the highest possible entry pressure $p_{ent} = 6.5 \cdot 10^5$ Pa. The overpressure was measured at the entry (exit) collector and along the length of the model at certain cross sections with a maximum error of ±(3-5)% using piezometric tubes or master manometers. For flow visualization, models No. 16 and 17 were prepared from milled polymethylmethacrylate (PMMA) and after coating with MMMA the upper plate and side coverings were attached. During backlighting of the model from below, the flow pattern was visualized by the local introduction of ink into the channel. The images were fixed on film using a "Zenith-TTL" camera.

In order to generalize our results, we take as a characteristic dimension the hydraulic diameter of the channel d_h. One can use as a characteristic velocity the percolation velocity w_p, the mean velocity $w_2 = w_p\varepsilon^{-1}$, or the maximum velocity $w_1 = w_p\varepsilon\ell^{-1}{}_M$, where $\varepsilon = \varepsilon_M(2 - \varepsilon_M)$. The use of the velocity w_p is preferable when examining the waffled structure as a porous body, the use of w_1 when comparing with a channel system of coolers, and w_2 when studying the flow in one structure for various angles of attack γ. On the basis of these velocities we obtain the corresponding Reynolds numbers $Re_i = w_i d_h/\nu_\ell$ (with a maximum error of 5.0-6.0%), coefficients of hydraulic drag $\xi_i = \Delta p/[\rho w_i{}^2/2(d_h/l)]$ (with a maximum error of 10-15%). The indirectly measured values are determiend with a 0.95 confidence level.

For the in-step waffle structure (model No. 16), we carried out visualization for velocities which were characteristic for laminar flow ($120 < Re_1 < 650$). Each sequence had from one to several features, as a result of whose generalizations we can draw the following conclusions. For small Re ($Re_1 \simeq 200$) the laminar flow regime was clearly exhibited, and jet streams were clearly visible. There were symmetric cylindrical vortices of nearly perfectly straight form in the interfin spaces. But the flow was sensitive to small disturbances, in whose capacity small pressure nonuniformities at the entry–exit (caused by gas bubbles, for example) could serve, as could imperfections in the geometry of the structure. Therefore we observed in the dynamics the transformation of vortices from two symmetric vortices to two cone-shaped vortices (in space) with periodic changes in the position of the cone vertex from one unfinned surface to another for every vortex. We visualized the formation of boundary layers at the leading edges of the fins, constriction of the basic flow in the interfin space and its expansion in the free space.

Upon increasing Re_1 to 400 there began "braided" flow, which was especially marked at the initial injection of dye into the device. It was characterized by a periodicity over two longitudinal spacing sof the structure. The formation of braids was evidently connected with the formation of a secondary flow similarly to channels with right-angle profiles [3]. Subsequent increase in the velocity led to intermittant flow.

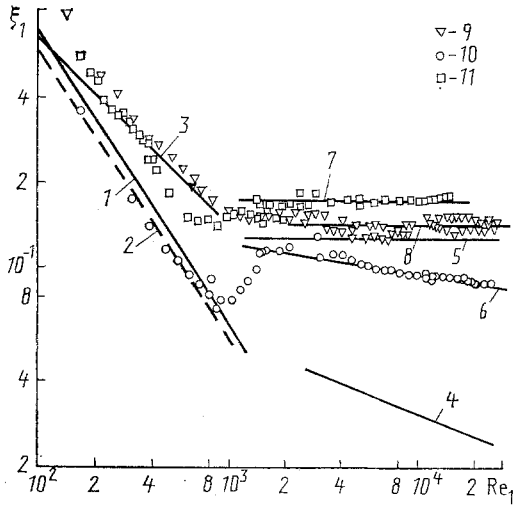

Fig. 2. Dependence of the coefficient of hydraulic drag ξ_1 on Reynolds number Re_1 for in-step structures: 1) $\xi_1 = 64/Re_1$; 2) $\xi_1 = 56.6/Re_1$ ($h_c/\delta_c \approx 0.9$); 3) formula (5); 4) $\xi_1 = 0.316/Re_1^{0.25}$; 5) formula in [7]; 6) formula (6); 7) approximation, $\xi_1 = 0.173$; 8) approximation, $\xi_1 = 0.14$; 9) experiment, Model No. 1; 10) experiment, model No. 3; 11) experiment, model No. 12.

For a square staggered structure (model No. 17), we carried out visualization for $70 \leq Re_1 \leq 2300$. We observed laminar meandering flow for $Re_1 \leq 70$, with stagnated regions forming behind the fins. The streamlines remained laminar and meandering for an approximately two-fold increase in velocity ($Re_1 \approx 130$). We noted the beginning of vortex formation in the afterbody zones of the fins. Despite the fact that fluid molecular diffusion was weak and turbulent diffusion nonexistent, the dye spread rapidly through the transverse section of the model. With subsequent velocity increase ($Re_1 = 190$), the break-away pattern of the vortices from the fin edges resembled the Kármán vortex trail which forms in the flow about a cylinder [4]. The transformation to the inertial flow regime begins, which occurs at the start of turbulence development. Subsequent ($Re_1 > 250$) flow loses the meandering traits and acquires a convergent–divergent flow character. There is rapid (2-3 rows) spread of contaminants at all sections of the model, the concentration patterns being similar to one another and depending only weakly on the flow velocity. This is indicative of the decisive influence of cooling system structure on the spread of contaminants. By means of a probabilistic approach [5], contaminant concentrations were computed in the transverse sections. These agreed well with the results of the photometric records. Visualization allowed the authors to construct flow diagrams and to substantiate a number of hypotheses on the development of methods for computing the drag coefficients.

The hydraulic drag coefficients for waffled structures have been determined over a wide range of Reynolds numbers ($50 < Re_1 < 2.5 \cdot 10^4$) (Figs. 2-4). Since the in-step waffle system is in a certain sense basic (the other flow cases correspond to its flow at angles of attach γ), we examine its hydraulic drag in detail (Fig. 2).

The in-step structures of models No. 1, 3, 6, and 12 were distinguished by individual features which affected the behavior of the relation $\xi_1 = f(Re_1)$ in all regions of the flow. In these models, the stages of viscous flow were clearly expressed right up to $Re_1 \approx 950$, but system No. 1 had roughened walls, which led to the earliest (in Reynolds number) deviation from the relation $\xi_1 \sim Re_1^{-1}$ (at approximately $Re_1 \approx 400$) and to the switch to similarity in practice for $Re_1 \geq 10^3$ ($\xi_1 = 0.14$). The difference in system No. 12 ($\varphi = 60°$) consisted of a later onset of the flow transition zone, which is more extended ($600 \leq Re_1 \leq 1400$) and which has a modest minimum. For $Re_1 > 1.4 \cdot 10^3$, the similarity stage of the flow begins at $\xi = 0.173$, which is explained by the rhombic form of the fins. Systems No. 3 and 6 were prepared by milling, which produces smoother surfaces, and the behavior of their drag coefficients in the region of turbulent Reynolds numbers ($Re_1 > 1.6 \cdot 10^3$) differs fundamentally from models No. 1 and 12. By statistical manipulation of the results using the method of least squares we obtained, for this region, the relations (ignoring dispersion) for models No. 3 and 6, respectively:

$$\xi_1 = 0.228\,\mathrm{Re}_1^{-0,093}, \tag{2}$$

$$\xi_1 = 0.3\,\mathrm{Re}_1^{-0,120}. \tag{3}$$

In the region of laminar Re_1, the results were split: For $Re_1 < 950$ for model No. 3 they were close to the classical relations for a cylindrical pipe ($\xi = 64\ Re_1^{-1}$) and for a right angled channel with a side ratio of $h_c/\delta_c \approx 0.9$ ($\xi_1 = ARe^{-1}$, A = 56.6 [6]). For model No. 6 and $Re_1 < 500$, the experimental points were best described by the relation $\xi_1 = 76\ Re_1^{-1}$. For this model and $Re_1 > 500$ a transitional flow occurs with a weakly expressed minimum in the range $900 < Re < 1\cdot10^3$. Subsequently, ξ_1 increases up to $\xi_1 = 0.13$ for $Re_1 = 1.6\cdot10^3$, then diminishes in accordance with (3) for $Re_1 > 1.6\cdot10^3$. Compared to turbulent flow in smooth pipes ($\xi_{sm} = 0.316\ Re^{-0.25}$), the flow in smooth waffled structures is characterized by large drag coefficients: $\xi_1/\xi_{sm} \approx 2.5$ ($Re_1 = 2.5\cdot10^3$) and $\xi_1/\xi_{sm} = 3.6$ ($Re_1 = 2\cdot10^4$).

Applying the relation for in-line tube bundles [7] to our relative dimensions gives the value $\xi = 0.125$ (for $\bar{S}_2 \gg 2$) for $10^3 < Re < 10^4$, which agrees well with the drag in models No. 1, 3, and 6 (for $1.6\cdot10^3 < Re_1 < 2.5\cdot10^3$).

For $10^4 < Re_1 < 2\cdot10^5$, a mixing flow region is established for tube bundles and the drag relation acquires a power-law character [7]: $Eu_z = ab\ Re^r$, where $a = 0.26$, $b = f(\bar{S}_2, \bar{S}_1)$, and $r = -0.12[(\bar{S}_2 - 1)/(\bar{S}_1 - 1)]^{0.5}$. Considering the relation between Eu and ξ [$\xi = 2Eu_z d_h/(\delta_c + \delta_f)$], we obtain the formula ($\bar{S}_2 = \bar{S}_1 = 2$)

$$\xi_1 = (0.34 - 0.36)\,\mathrm{Re}_1^{-0,12}, \tag{4}$$

which agrees well with the drag in models No. 3 and 6 [formulas (2) and (3)] for $Re > 1.6\cdot10^3$ and $a = 0.22$. These examples indicate a definite correlation between bundles and waffled structures.

We have attempted to generalize our results, using the hypothesis of superposition of drag [8]. For in-step waffle structures in the laminar Re_1 region we have obtained the drag as a sum of friction on the unfinned plate surfaces and the side surfaces of the fins and the pressure loss in the interfin space, connected with the vortex unwinding in the "umbral" zone and with velocity profile restructuring upon fluid entry between the fins:

$$\xi_\Sigma = \frac{A}{\mathrm{Re}_1}\left(\frac{d_h}{2h_c}\right)^2 + K_p\frac{d_h}{l} + \frac{(3.4-4.0)}{\sqrt{\mathrm{Re}_1}}\left(\frac{d_h}{\delta_f}\right)^{1.5}, \tag{5}$$

Here the third term in ξ_Σ contributes 50-70% of the total sum. Formula (5) successfully generalizes the experimental points over the range $100 < Re_1 < 500$ for models No. 1, 6, and 12 (Fig. 2).

A turbulent boundary layer develops at the unfinned walls in the turbulent flow region, and in the interfin spaces jet flow occurs. From analysis based on [8, 9] and on the coefficient of hydraulic drag for roughened walls ξ (R_z, Re_1) [3], we obtain

$$\xi_\Sigma = \frac{\delta_c}{(\delta_c + h_c)}\xi(R_z,\ \mathrm{Re}_1) + 2.28\frac{C\delta_c}{d_0} - 2.24\left(\frac{C\delta_c}{d_0}\right)^2, \tag{6}$$

where C is a constant characterizing the degree of turbulence and nonuniformity of the flow velocity field [9] and $d_0 = 1.13\ (\delta_c h_c)^{0.5}$.

From (6) it follows that ξ_Σ is in practice similar to Re_1, and the jet effect contribution amounts to 80-90%. By singling out the effect of the angle of attack γ, we succeeded in representing the results for groups of the same types of models (Nos. 1-5, Nos. 6-10, and Nos. 11-15) in ξ_2, Re_2 coordinates (Figs. 3, 4). Increasing the angle of attack for models No. 6-10 (Fig. 3) leads to rapid growth of the drag to a maximum at $\gamma = 45°$ ($\varphi = 90°$); relative to $\gamma = 0°$, it grows by a factor of 12-16. The power exponent on Re in this case increases from −0.12 to 0. Due to the error in determining ξ_2 we were not always successful in finding this exponent, since the change in the value $Re_2^{n_0}$ does not exceed the error limits in the Re_2 range considered here. Therefore, we adopted a similarity rule with respect to the Reynolds number for $\gamma \geq 15°$, that is, when the drag on the form begins to predominate

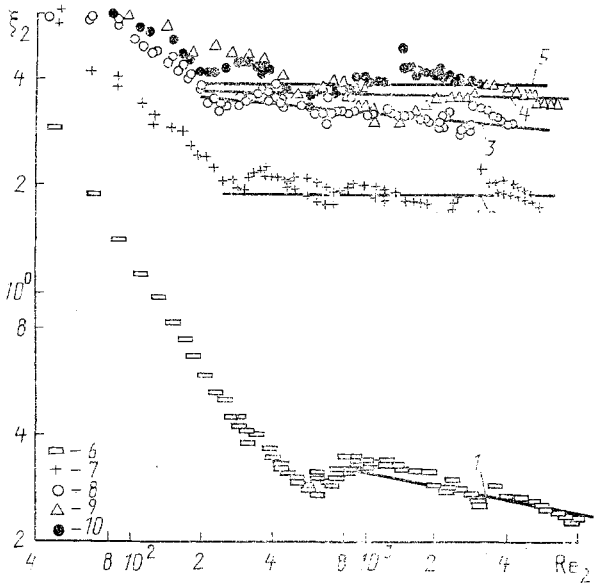

Fig. 3. Dependence of the coefficient of hydraulic drag ξ_2 on Reynolds number Re_2 for models No. 6-10 (φ = 90°): 1-5) approximation: 1) $\xi_2 = 0.72\ Re_2^{-0.12}$; 2) $\xi_2 = 1.9$; 3) $\xi_2 = 4.74 \cdot Re_2^{-0.06}$; 4) $\xi_2 = 3.6$; 5) $\xi_2 \simeq 4$; 6-10) experiment: 6) model No. 6; 7) model No. 7; 8) model No. 8; 9) model No. 9; 10) model No. 10.

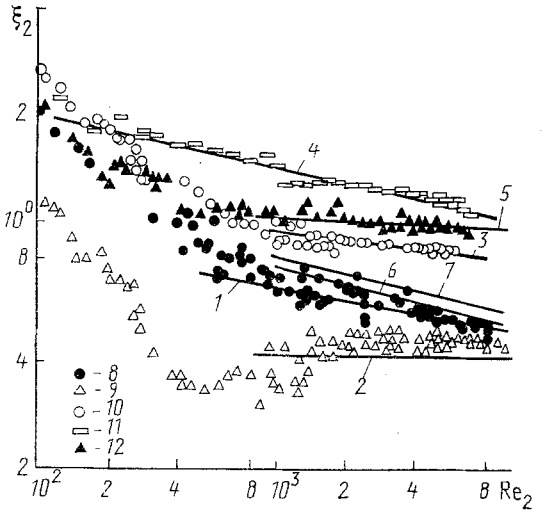

Fig. 4. Dependence of the coefficient of hydraulic drag ξ_2 on Reynolds number Re_2 for models No. 11-15 (φ = 60°): 1-5) approximation: 1) $\xi_2 = 2.12\ Re_2^{-0.164}$; 2) $\xi_2 = 0.41$; 3) $\xi_2 = 1.7\ Re_2^{-0.08}$; 4) $\xi_2 = 3.14\ Re_2^{-0.12}$; 5) $\xi_2 = 1.2\ Re_2^{-0.022}$; 6) formula (7) for model No. 11; 7) formula (7) for model No. 13; 8) experiment, model No. 11; 9) experiment, model No. 12; 10) experiment, model No. 13; 11) experiment, model No. 14; 12) experiment, model No. 15.

over the friction drag by a factor of five or more. The onset of the inertial flow regime with growing γ shifts to smaller Re_2; in model No. 6 (γ = 0°) the transition to the viscous–inertial regime occurs for $Re_2 \simeq 600$, in model No. 7 (γ = 15°) at Re_2 = 300, and in models No. 8-10 (γ = 30, 40, 45°) at Re_2 = 250-200. For $Re_2 < 200$, $\gamma \geq 30°$, the ξ_2 coincide and change proportionally to $Re_2^{-0.5}$, which differs from model No. 6 ($\xi_2 \sim Re_2^{-1}$). Similarly in dependence on γ and drag also changes in models with large structural dimensions (models No. 1-5, d_h = 2.0-2.4 mm), the transition to the viscous–inertial regime is observed for $Re_2 < 200$ ($\gamma \geq 15°$). For this group of models the results on hydraulic drag were obtained

by the method of Il'in [10] ($\Delta p/l = \alpha\mu w_p + \beta\rho w_p^2$). The viscous coefficient α and the inertial coefficient β for the hydraulic drag were determined by considering the waffled structure as a pseudo-porous medium.

The change in hydraulic drag is quite singular for decreasing φ (models No. 11-15) (Fig. 4). Despite models No. 11 and 14 having staggered structure with roughened walls (a result of electro-machining technique), we observed a decrease in ξ_2 in these models with growth in Re_2. Model No. 13 had relatively smooth walls (comapred to Nos. 11 and 14), but in this case the exponent on Re_2 was larger. Using the most dense staggered structures ($\bar{S}_1 = S_1/\delta_f = \bar{S}_2 = 1.5$ for model No. 15, $\bar{S}_1 = \bar{S}_2 = 1.67$ in model No. 13 and $\bar{S}_1 = \bar{S}_2 = 2$ in models No. 11, 12 and 14) leads to an increase in drag which qualitatively agrees well with the rules for tube bundles [7]. For $\varphi = 90°$ we did not observe such agreement. Here ξ_2 also grows with increasing γ, but to a much reduced extent compared to the case $= 90°$. So, for example, the drag in model No. 14 ($\gamma = 30°$) compared to model No. 12 is larger by a mere factor of 3.5-2.5 ($10^3 < Re_2 < 7\cdot10^3$).

The formula for the drag on staggered tube bundles situated in an equilateral triangular grid over the Reynolds number interval $6\cdot10^2 < Re_1 < 7\cdot10^3$ [7] as applied to our structures has the form

$$\xi_2 = 0.71\,(\bar{S}_1 - 1)^{-0,33}\left(\frac{2d_h}{\delta_c + \delta_f}\right)\left(\frac{\varepsilon}{\varepsilon_M}\right)^2\left(\frac{\varepsilon}{\varepsilon_M}\mathrm{Re}_2\right)^{-0,15}. \tag{7}$$

For model No. 11 ($\bar{S}_1 = 2$), using (7) and an approximation to the experimental data, respectively, we obtain

$$\xi_2 = 2.16\,\mathrm{Re}_2^{-0,15}, \tag{8}$$

$$\xi_2 = 2.12\,\mathrm{Re}^{-0,164}\ (10^3 \leqslant \mathrm{Re}_2 < 10^4), \tag{9}$$

which are satisfactorily consistent with one another (see Fig. 4).

For models No. 13 and 15, (7) gives satisfactory agreement for Re_2 close to the lower bound of the interval $10^3 \leq Re_2 \leq 10^4$. We obtain better quantitative agreement with experimental results for the smooth walled structures over full range of Re_2 if in (7) we introduce the term $(\bar{S}_1 - 1)^{-0.5}$ in place of $(\bar{S}_1 - 1)^{-0.33}$.

The effect of the angle on the drag for models No. 1-5 is found through its influence on the inertial coefficient of the hydraulic drag β [10] (see the formula given above for $\Delta p/l$):

$$\bar{\beta}_\gamma = \beta_\gamma/\beta_{45} = \bar{\beta}_0^{1-\bar{\gamma}} = 0.0823^{1-\bar{\gamma}}, \tag{10}$$

where $\bar{\beta}_0 = \beta_0/\beta_{45}$, $\bar{\gamma} = \gamma/45$ ($0 \leq \bar{\gamma} \leq 1$), and the index on β corresponds to the angle of attack.

Calculations using (10) require knowledge of β for two extreme values of the angle of attack γ: for in-step and for staggered structures. We can immediately obtain the relation $\xi_2(\gamma)$ by comparing the values of ξ_2 for fixed Re_2. Such a method is useful for similarity of ξ_2 to changing Re (or where friction makes a small contribution). So, for models No. 6-10 we obtain the empirical equation

$$\xi_2 = 0.072\,(\gamma + 10)\ (15 \leqslant \gamma < 45°). \tag{11}$$

Considering the staggered structures (models No. 2 and 10) as an aggregate of periodically repeating plane convergent–divergent elements demonstrates that in the turbulent flow regime there is a regime of complete flow separation in the divergent sections (which is supported visually) and hydraulic loss must in practice consist of the loss upon expansion [1]

$$\xi_e = 3.2\,(\mathrm{tg}\,\varphi/2)^{1,25}, \tag{12}$$

where ξ_e is computed using the velocity and hydraulic diameter in the narrow part of the structure. Then (120 for our case ($\varphi = 90°$) gives $\xi_e = 3.2$, and for $Re_1 > 300$ the deviation of this relation from the experimental data does not exceed 20% (the equation being too low compared to the data points).

Conclusions. Thus the experimental results obtained and their generalization allow us to compute the drag coefficients in cooling systems with intersecting channels of modest relative height, which can be used as a basis for construction of energy plant elements and for optimizing them.

NOTATION

d_h is the hydraulic diameter of the channel, $d_h = 4F_c/P_c$; F_c, P_c are the area and perimeter of the channel; h_c is the channel height; R_z height of roughness element; φ is the angle of intersection of the channels; γ the angle of attack; δ_c is the channel width; δ_f the fin thickness; S_1, S_2 are the transverse and longitudinal channel spacings; ε is the porosity, the ratio of the void volume to the total volume of an elementary cell of the cooling system; $K = 4/\delta_f - 2\varepsilon\,(2/\delta_f - 1/h_c)$ is the compactness of the cooling system, that is, the ratio of the heat exchange surface area to the volume of the elementary cell; Δp is the pressure drop over the distance ℓ between pressure samplings; w is the fluid velocity; α, β are the viscous and inertial coefficients of the hydraulic drag for a porous body [10]; ρ, μ are the fluid density and dynamic viscosity; K_p is a coefficient which accounts for the pressure loss at the initial element [11]; ξ is the coefficient of hydraulic drag; $\xi(R_z, Re_1) = \{1.74 - 2\log[2R_z/d_h + 1.87/(Re_1\sqrt{\xi(R_z, Re_1)})]\}^{-2}$ is the hydraulic drag coefficient for roughened walls [3]; Re is the Reynolds number; Eu_z is the Euler number scaled for one series of structures.

LITERATURE CITED

1. I. E. Idel'chik, Hydraulic Drag Handbook [in Russian], Moscow (1975).
2. V. V. Kharitonov, Thermophysical Analysis of Laser Mirrors [in Russian], Moscow (1985).
3. G. Schlichting, Boundary Layer Theory [Russian translation], Moscow (1974).
4. M. van Dyke, Album of Flow in Fluids and Gases [Russian translation], Moscow (1986).
5. A. N. Kolmogorov, Mathematics: Science and Profession [in Russian], Moscow (1988).
6. I. L. Povkh, Technical Hydrodynamics [in Russian], Leningrad (1976).
7. A. Zhukauskas, V. Makaryavichyus, and A. Shlanchyauskas, Heat Transfer for Tube Bundles in Fluid Crossflow [in Russian], Vilnius (1968).
8. M. D. Millionshchikov, Turbulent Flow in Boundary Layers and in Pipes [in Russian], Moscow (1969).
9. R. G. Bogoyavlenskiĭ, Hydrodynamics and Heat Exchange in High-Temperature Atomic Reactors with Spherical Fuel Elements [in Russian], Moscow (1978).
10. S. V. Belov, Porous Metals in Industrial Engineering [in Russian], Moscow (1981).
11. A. A. Zhukauskas, Convective Transfer in Heat Exchangers [in Russian], Moscow (1982).